Vacuum 146 (2017) 509–516

Contents lists available at ScienceDirect

Vacuum

journal homepage: www.elsevier.com/locate/vacuum

Effect of the seed layer on the growth and orientation of the ZnO nanowires: Consequence on structural and optical properties

A. Serrano [a], A. Arana [a], A. Galdámez [a], A. Dutt [a], B.M. Monroy [a], F. Güell [b], G. Santana [a, *]

[a] Instituto de Investigaciones en Materiales, Universidad Nacional Autónoma de México, Coyoacán, México City, 04510, Mexico
[b] Departament d'Enginyeries: Electrònica, Universitat de Barcelona, C/Martí i Franquès 1, E-08028 Barcelona, Catalunya, Spain

ARTICLE INFO

Article history:
Received 1 November 2016
Received in revised form
1 March 2017
Accepted 5 March 2017
Available online 7 March 2017

Keywords:
ZnO
Seed layer
Ultrasonic spray pyrolysis
Sputtering
Luminescence

ABSTRACT

High quality vertically aligned zinc oxide (ZnO) nanowires (NWs) were grown on Au-coated aluminum-doped zinc oxide (AZO) thin films via vapor-liquid-solid (VLS) technique. AZO seed layers were deposited using two different techniques named as ultrasonic spray pyrolysis (USP) and magnetron sputtering. Structural, morphological and compositional properties of the NWs grown on the two distinct seed layers were analyzed in detail by using X-ray diffraction (XRD), scanning electronic microscopy (SEM) and energy dispersive spectroscopy (EDS) techniques, respectively. In the first case, (seed layer grown by USP technology), NWs showed the (101) orientation, whereas in the second case, (seed layer grown by sputtering) NWs showed (002) orientation. It was confirmed by the SEM images, that NWs with (002) orientation shown better vertical alignment than NWs with (101) orientation. In addition, optical properties were also studied using photoluminescence (PL) spectroscopy and irrespective of the preferred orientation, NWs showed a strong green emission at room temperature. The study made in the present work on the seed layer preparation by two techniques and hence, deposition conditions to achieve fully controllable ZnO nanowires with precise distance, shape, position and orientation could provide opportunities for the fabrication of future optoelectronic devices.

1. Introduction

Among different form of nanostructure materials, one-dimensional (1-D) nanomaterials, especially, nanowires (NWs) are of particular attention because of their potential applications in developing novel electronic, optoelectronic devices due to effective confinement of carriers and photons on a high surface to volume ratio [1,2]. Regarding dimensions, starting from less than 100 nm, they could reveal a non-confined axis that may reach up to microns scale [3–5]. This particular property is critical for an efficient charge transport mechanism in applications like solar cells [6,7]. Between various investigated materials for NW growth, ZnO is one of the vastly explored sources due to better structural, optical and electrical properties.

ZnO is an II-VI semiconductor with a wide direct band gap in the near ultraviolet (UV) (Eg = ~3.3–3.37 eV at 300 K) and exhibit a large exciton binding energy (60 meV) ideal for excitonic emission at room temperature [8–10]. ZnO crystallizes in two main crystalline structures: hexagonal wurtzite and zinc blend. Under general conditions, it exhibits a hexagonal wurtzite with lattice parameters a = 0.32469 and c = 0.52069 [1,8]. However, at high-pressure conditions (~10 Gpa) a third crystalline structure (rock salt) can also be found [9,11–13]. ZnO is considered as a versatile material which can exists in a diverse group of morphologies, such as nanobelts [12,14–16], nanocages [14], nanowires [17–19], nanorings [12,14], core-shell structures, nanorods [12,14–16], nanosheets [15], nanoflowers [15], nanoneedles [20]. It exhibits near-UV emission, good conductivity, transparency, high-temperature electronic degradation, high radiation resistance and biocompatibility [1,21]. Above mentioned features together make ZnO an ideal material for diverse applications.

Additionally, ZnO nanowires are one of the most important nanomaterials in today's research. In specific, vertical-aligned ZnO nanowires are regarded as promising candidates for various applications like UV laser [6,8], LED's [21], solar cells [22], gas and piezoelectric sensors and photocatalysis reactions [23–25]. A large number of physical and chemical methods have been applied and investigated for the growth of these nanostructures. Most of the approaches make use of bottom-up routes that offers the possibility

* Corresponding author.
E-mail address: gsantana@iim.unam.mx (G. Santana).

http://dx.doi.org/10.1016/j.vacuum.2017.03.010
0042-207X/

for a controlled growth of the NWs with the well-desired and defined aspect ratio [26]. Methods such as chemical vapor deposition (CVD) [20,27], metal-organic chemical vapor deposition (MOCVD) [21,27], flame transport processes [24,28], sol-gel [29], physical vapor deposition (PVD) [20,27,30], molecular beam epitaxy (MBE) [21], pulsed laser deposition (PLD) [1,27], vapor-liquid-solid (VLS) [22,31,32], sputtering and solution-based methods [22,30] have been used to grow ZnO NWs.

Amongst all of the methods mentioned above, VLS also called as metal catalyzed method, is one of the most important in the growth of 1-D nanostructures, especially NWs [16,30]. The process involves the use of a catalyst (in the form of nanoparticles) that forms a eutectic alloy with the substrate or with the seed layer [16,31,33]. Gaseous reactants dissolve into the liquid droplet leading to a supersaturated solution that facilitates nucleation and finally, leads to the growth of the NWs (Fig. 1a) [15,16,27]. NWs growth continues until the source material is either finished or if the surface/growth temperature is reduced [27,31]. Moreover, using VLS method heterostructures could also be obtained by changing the reactants source [34]. Light emission from well-known semiconductor materials like Si, GaAs, and GaP has already been studied and explained in depth. Nevertheless, as mentioned above, attracting properties of ZnO nanowires are now considered as an interesting additional material, which could be used for optoelectronic applications.

To date, there exist some reports where it is demonstrated the growth of ZnO NWs by using various methodologies and further, optical properties of NWs has been explored. Recently, some of the researchers have grown ZnO nanowires using a single zone CVD system, and they have observed a strong PL emission at 3.23 eV, which was attributed to recombination of free excitons [35]. On the other hand, they observed a very low emission in the green-yellow region. In the other recent report, authors studied the effect of the seed layer on the growth and UV detection properties of ZnO NWs [36]. On the other hand, in another old report, it was demonstrated the growth of ZnO 1D micro and nanostructures by using MOCVD at atmospheric pressure, and PL, in that case, was observed at around 3.3 eV [37]. Also, they explained that using VLS technique, the growth of gold catalyst should start above 900 °C. In other previous report, authors grew ZnO nanowires on a pre-coated ZnO epilayer, and the emission at 3.26 eV was correlated with the recombination of free excitons. While a broad green emission at 2.48 eV was attributed to surface defects at room temperature [38].

In another previous article, ZnO NWs were grown using AZO seed layer by using aerosol deposition method [39]. In that article, authors were able to synthesize NWs, which were randomly distributed, and only one PL peak in UV region was observed. Also, in another previous report, the effect of the seed layer on the structural properties of ZnO NWs has been explained in detail [40]. However, detailed study on the control over the growth and hence, the orientation of ZnO NWs grown using different kind of seed layers with their particular effect on the photoluminescence emission is one of the left over constraints. Control over morphology by controlling the deposition parameters could help to enhance the application point of view of ZnO NWs.

In the present article, foremost we present a versatile comparison of high-quality ZnO NWs grown on two distinct seed layers subsequently grown by two different techniques such as ultrasonic spray pyrolysis and magnetron sputtering methods without any need of template method for the growth mechanism. Furthermore, depending on the seed layer and deposition technique, control over the aspect ratio and alignment of the nanowires has been shown. For obtaining a new generation of optoelectronic devices, work reported in this article could provide vital information about the various deposition conditions and film properties that could further allow the precise control over the distance, shape, density, position and orientation of the ZnO nanowires. The method and study presented here, shown the growth of ZnO NWs with a diameter varying from 30 to 70 nm and length up to 7 μm which could be used in a variety of applications. Additionally, bright green emission demonstrated in the present work could also reinforce the utilization of the present material for widening the active spectral region of ZnO-based optoelectronic devices and/or for downshifting process in photovoltaics.

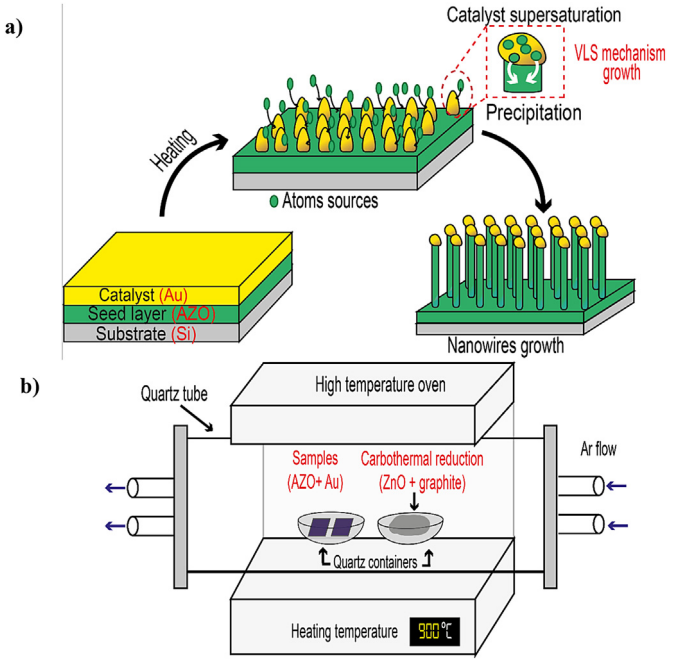

Fig. 1. a) Basic principle of the VLS growth mechanism of ZnO NWs and b) Scheme showing the High-temperature treatment employed for NWs growth at 900 °C using a mixture of ZnO powder (as atoms source) and graphite (as carbothermal reduction).

2. Experimental

2.1. Materials

2.1.1. Ultrasonic spray pyrolysis

For ultrasonic spray pyrolysis, salts of zinc acetate dehydrate ($ZnC_4H_6O_4{}^*2H_2O$) as zinc atoms precursor and aluminum acetylacetonate ($Al(C_5H_7O_2)_3$) as dopant atoms were employed. A mixture of methanol (CH_3OH) and deionized water (84.6% and 15.4%, respectively) was used as a solvent. Acetic acid ($C_2H_4O_2$) was used to improve the solubility of the salts in the precursor solution.

2.1.2. Magnetron sputtering

On the other hand, for sputtering process a zinc oxide solid target (size: 2″ diameter x 0.125″ thickness) and with alumina at 2 wt. % (PLASMATERIALS®) was employed. Argon gas (99.999%) was used to generate the plasma in the sputtering process, and water was employed as a coolant during the deposition process.

2.2. Substrate preparation

Silicon and quartz substrates (25 mm × 10 mm) were used in both of the deposition techniques. Substrates were cleaned up before deposition to avoid impurities that could affect the final product. Trichloroethylene (CHCl: CCl_2), acetone ($(CH_3)_2CO$), and isopropyl alcohol (C_3H_8O) were used separately in ultrasonic baths

(5 min per bath) to remove any rest of grease in both silicon and quartz substrates. After each bath, pressurized nitrogen (N_2) was used to dry out the samples.

2.3. Seed layer deposition method

2.3.1. Ultrasonic spray pyrolysis

As mentioned in section 2.1.1, the precursor solution was made using a mixture of 0.1 M of zinc acetate and 4.45 at. % of aluminum acetylacetonate diluted in 100 mL of a methanol (84.6%) and deionized water (15.4%), respectively. 0.5 mL of acetic acid was added to improve the solubility of the salts in the precursor solution. The solution prepared was stirred for an hour. A set of resistors, controlled by a temperature controller, were used to heat the tub. The precursor solution was placed in a dropping funnel through where finally it was introduced to the nebulization chamber. The role of the nebulizer was to form tiny drops of the precursor solution. The nebulization gas set up in this stage was carried to the synthesis chamber by a carrier gas (compressed air) and was directed to the substrates using a director gas. The deposition process was carried out at a temperature of 475 °C for 17 min with controlled fluxes of 0.642 L/min and 2.564 L/min for carrier and director gas sources, respectively.

2.3.2. Magnetron sputtering

A magnetron sputtering system was employed to deposit AZO thin films on both silicon and quartz substrates. The substrates-target distance was set to a value of 4 cm for the deposition process. Mechanical and turbomolecular bombs were employed to achieve high vacuum (9.3×10^{-5} mbar) inside the deposition chamber. After achieving the required pressure, the chamber was filled up with Ar gas, until; it got a pressure of 1.2×10^{-2} mbar. Before opening the shutter, a cleaning process (approximately 5 min) was employed to remove remaining impurities from the target's surface to avoid possible contamination of the final products. The power source was maintained at 40 W for the duration of 60 min for the growth of AZO thin films.

2.3.3. Catalyst deposition

After the deposition of the AZO seed layers, via USP and magnetron sputtering, samples were covered with a 4 nm of gold (Au) thin layer. Cressington Scientific DC Sputter unit was used for sputtering. Ted Pella® Au target (57 mm diameter and 0.1 mm thickness) was used to deposit the catalyst layer.

2.4. Nanowires growth

Finally, after the deposition of the AZO seed layers and the Au catalyst layer, NWs growth takes places at this stage. A high-temperature oven, HAT-1200 from EVELSA, with a quartz tube inside was employed for NWs growth. Fig. 1b demonstrates that two quartz containers were placed inside the quartz tube. One of quartz container contains the samples with seed AZO layers and Au catalyst, and the other one contains the mixture of ZnO powder (99.999%) as Zn source and graphite (99.99%) for carbothermal reduction as mentioned earlier.

The VLS process was carried out at 900 °C in an Ar environment for 60 min, and finally, the sample was cooled to room temperature for the duration of 10 h.

2.5. Characterization techniques

Structural, morphological, chemical composition and optical properties of the thin films were analyzed by different characterizations techniques in order to collect information at each stage of the NWs growth (from seed layer deposition to the final development of the ZnO NWs).

For structural characterization, X-Ray Diffraction (XRD) RIGAKU Ultima IV equipment using a copper (Cu) anode with K_α line of 1.5418 Å was used. Measurements were performed in the grazing incidence angle mode ($\omega = 2°$) with 2θ angle varying from 25 to 65° at step of 1° in 1 min. Finally, results were corroborated using zincite (COD 96-900-4180) and gold (COD 96-901-3045) database sheets.

Morphological properties were studied using a field emission scanning electron microscopy (FESEM) in a JEOL JSM-7600F equipped with a Schottky emitter electron source. Images of planar and cross-sectional modes were obtained at different resolutions (100,000x, 50,000x, 25,000x, and 10,000x) using secondary electron image (SEI), lower-secondary electron image (LEI) and low-angle backscattered electrons (LABE) detectors. Images obtained were processed in specific software to get some statistic information about diameter and length of the grown NWs. Energy dispersive spectroscopy (EDS) measurements were performed in parallel to SEM measurements to get some information about the compositional analysis.

Null (zero) ellipsometry, using a Gaertner L117 ellipsometer, was employed to obtain the information about the refractive index of the samples, especially, the ones with the seed layers. Also, photoluminescence (PL) measurements were performed on the samples using a He-Cd laser with a 325 nm excitation wavelength and 25 mW of power at room temperature. With the utilization of a UV lamp (λ-366 nm), the luminescence of samples was also recorded at the room temperature with a normal camera.

3. Results and discussion

3.1. Structural properties

Fig. 2 shows the XRD patterns for seed layers deposited via USP and sputtering techniques, respectively. USP-deposited layer showed polycrystalline feature, whereas, on the other hand, sputtering-deposited seed layer shown less crystalline feature. This structural difference could be related to the deposition parameters, growth conditions and working principle of both techniques. For instance, substrates in USP deposition were constantly heated at

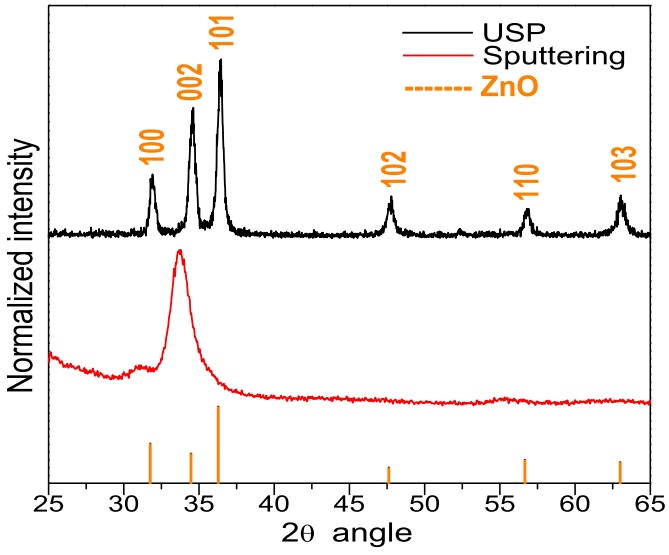

Fig. 2. XRD patterns of the USP and sputtering-deposited AZO seed layers using grazing incidence angle mode ($\omega = 2°$).

475 °C during the deposition time, while, in the case of sputtering deposition system they just got a minimal heating during the whole deposition process.

From Fig. 2 it can be observed that UPS-deposited sample showed the different orientations like (002), (100), (101), (102), (110) and (103) with the main orientation towards (101) peak (at around 34.6°). It is also seen that there is a slight shift to the right side of each peak in USP sample (on an average of 0.1° shift) and which could be related to the modification of ZnO lattice due to the incorporation of dopant atoms (Al atoms). In the case of sputtered sample, there is only a broad peak at near 33.78° corresponding to (002) plane. It must be noted that no secondary phases related to aluminum (e.g. alumina) were found in the patterns.

The difference in main diffraction peak is related to the particular deposition technique. For sputtered sample, the peak observed at (002) is linked to a c-oriented growth of the crystals (Fig. 3a) and is same as obtained early by Cui et al. [41]. On the other hand, for USP-deposited sample the main peak at (101) plane is related to the tilted (Fig. 3b) growth of the crystals.

After ZnO NWs growth, XRD characterization was another time performed on the samples. Fig. 4 shows XRD patterns of the samples after ZnO NWs growth. Patterns show a polycrystalline feature for both samples. Regardless of the NWs growth, samples maintain the same orientation peaks as in only the presence of AZO seed layer (Fig. 2). Additionally, patterns also shown particular peaks corresponding to the Au catalyst used for the growth of NWs (COD 96-901-3045 database sheet).

Grain size (G_s) of the crystals in the seed layers was obtained by using the Scherer's equation (equation (1)):

$$G_s = \frac{K\,\lambda}{\beta\cos(\theta)} \tag{1}$$

Where K is the shape factor (dimensionless with a value of 0.9), λ is the X-ray source wavelength, β is the light broadening at half maximum intensity (FWHM) in radians, Θ is the Bragg angle. Also, texture coefficient $\tau_{C(hkl)}$ using equation (2) was calculated from data obtained from XRD [44].

$$\tau_{C(hkl)} = \frac{I_{(hkl)}/I_{0\ (hkl)}}{\frac{1}{N}\Sigma_N\left(I_{(hkl)}/I_{0(hkl)}\right)} \tag{2}$$

Where, $I_{(hkl)}$ correspond to the measure relative intensity of a plane (hkl), $I_{0\ (hkl)}$ is the standard intensity taken from COD 96-900-4180 card and N is the diffraction number for the peaks.

Table 1 shows the results obtained from the calculations performed using equations (2) and (3). It can be seen that Gs of the seed layer deposited by the sputtering technique is smaller (about one third) compared to the Gs of the seed layer grown by USP. τ_c (*hkl*) values obtained are also shown in Table 1. Value of τ_c (*hkl*) close to the unity indicates that the number of crystals oriented in the (hkl) plane is in concordance with the datasheet. Whereas, values higher than the unity indicates that a specific (hkl) plane was promoted in the deposition technique. Calculations shows that (002) plane was promoted by USP deposition technique, while, main plane, (101), corresponding to ZnO kept closed to the unity. Despite of this increase, (101) peak in XRD pattern is still found to be more intense than (002) peak. In the case of the sputtering sample, calculation of T_c (*hkl*) was not possible due to the presence of only single wide peak found in the XRD pattern.

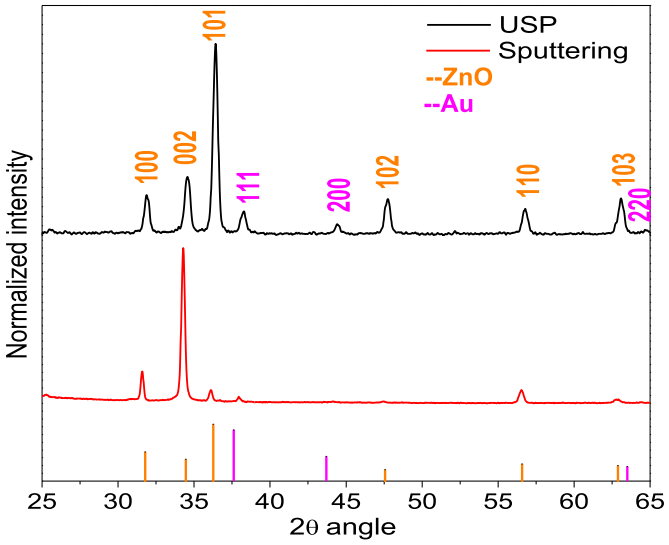

Fig. 4. XRD patterns of the samples after ZnO NWs growth using grazing incidence angle mode ($\omega = 2°$).

Table 1
Calculations of the grain size and texture coefficient of the seed layers obtained from XRD data.

G_s [nm]		$\tau_{C(hkl)}$	
RPU	Sputtering	RPU	Sputtering
17.8 (±2.7)	6.2 (±0.6)	$\tau_{C(100)} = 0.7$ $\tau_{C(002)} = 1.85$ $\tau_{C(101)} = 1.03$	–

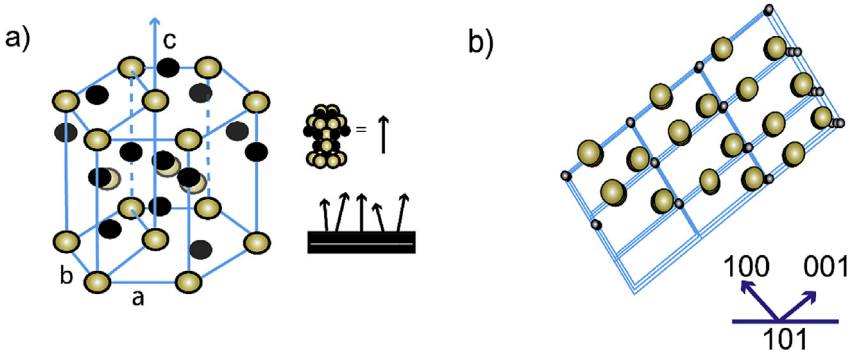

Fig. 3. Growing regimen of the crystals in ZnO thin film: a) c-oriented (columnar) growth [42] and b) tilted growth [43].

3.2. Morphological properties

Fig. 5 shows SEM images of AZO seed layers at 100,000-x resolution obtained using SEI detector. USP-deposited seed layer (Fig. 5a) shown well-packed grains (polycrystalline feature) compared with the sputtering-deposited sample (Fig. 5b). This result is consistent with the XRD patterns shown in Fig. 4, where it was observed that the sputtering-deposited seed layer showed less crystalline feature. All of the obtained results validate the fact that the temperature has a significant influence on the structural and morphological properties of deposited seed layers. Hence, thereby, it is quite understandable that the NWs growth could also be affected due to the changes observed in seed layer properties.

Identical to previous SEM characterization procedure, the same methodology was employed to characterize the samples after ZnO NWs growth. Fig. 6 shows SEM images of the NWs grown by VLS technique on Au-covered seed layers deposited via USP technique. Frontal view (Fig. 6a) shows the morphological structure of the ZnO NWs obtained after VLS growth; inset (Fig. 6b) achieved with LEI detector shows a difference in the contrast of NWs tip as in comparison to the rest of structure. The round-shaped structure at the tip corresponds to the Au catalyst (marked with yellow circles), whereas, the lengthened structure corresponds to the ZnO nanowire. Fig. 6c shows the cross-sectional image of the sample. It can be observed that the NWs growth is in a multidirectional way (zig-zag pattern). Obtained SEM results are in good concordance with results achieved in the XRD pattern.

On the other hand, in comparison to the ZnO NWs grown by USP on the Au-covered seed layer, NWs on the sputtering-deposited seed layer showed a high-ordered orientation (Fig. 7). In the planar view (Fig. 7a), hexagonal shape of the NWs is clearly visible. Similar to the other sample, here also in Fig. 7b round-shape structures corresponding to the Au catalyst could be observed. Unlike USP sample, this sample showed highly vertical oriented NWs. Results obtained are in consistence with the XRD spectra about the NW growth regime. The fact of finding the Au catalyst at the tip of the NWs validate that VLS growth mechanism directs the nanostructures growth on the seed layers deposited via USP and sputtering techniques.

More statistical studies were made on the obtained SEM images in the cross sectional mode, and the results are shown in Table 2. NWs grown by USP-deposited seed layer presented an average diameter (D) of 58.7 nm (±13.5 nm) and an average length (L) of 1.6 μm (±1.0 μm). On the other hand, sputtering-deposited seed layer sample presented an average diameter of 71.0 nm (±11.9 nm) and length of 3.1 μm (±0.4 μm). Apart from the visible morphological differences, these statistical analyses showed additional differences in the NWs grown by two AZO seed layers. NWs in the USP sample showed narrower diameter and shorter lengths compared to the sputtered sample. In addition, high statistical scattering of the data is found in USP sample as in comparison to the sputtered sample.

3.3. Chemical composition

Elemental composition of samples obtained from EDS spectra is also shown in Table 2. It is found there is a diminution in the oxygen (at%) for the sputtered sample compared to the USP one. Also, it can be observed that for the USP deposited sample, Al concentration is just about 15% of the total added precursor solution, but in the case of sputtered sample, Al concentration is not at all obtained. It can be assumed that in this case, the concentration incorporated to the

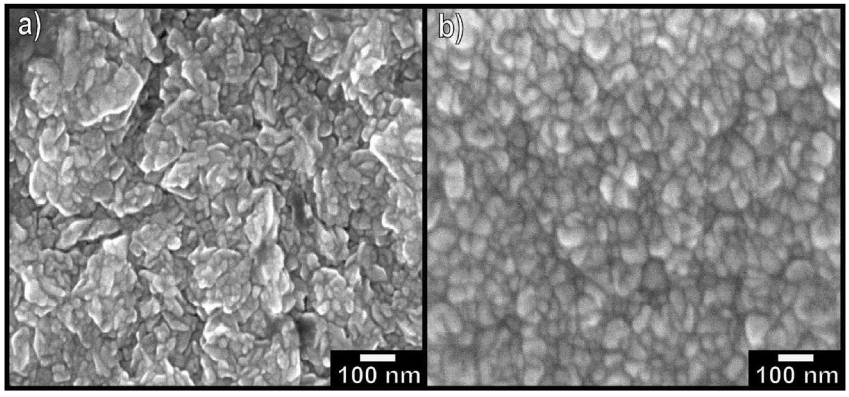

Fig. 5. SEM images of AZO seed layers using SEI detector at 100,000x resolution: a) USP-deposited layer and b) sputtering-deposited layer.

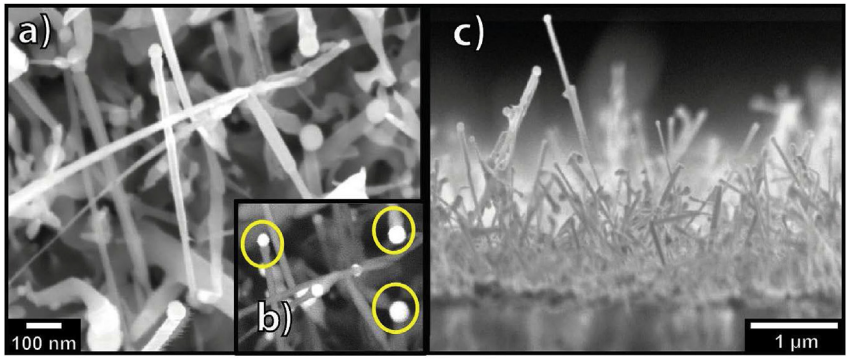

Fig. 6. SEM images of ZnO NWs grown on USP-deposited AZO seed layer (100,000x resolution): a) planar view (SEI detector), b) planar view (LEI detector) and c) cross-sectional view (SEI detector, 10,000x resolution).

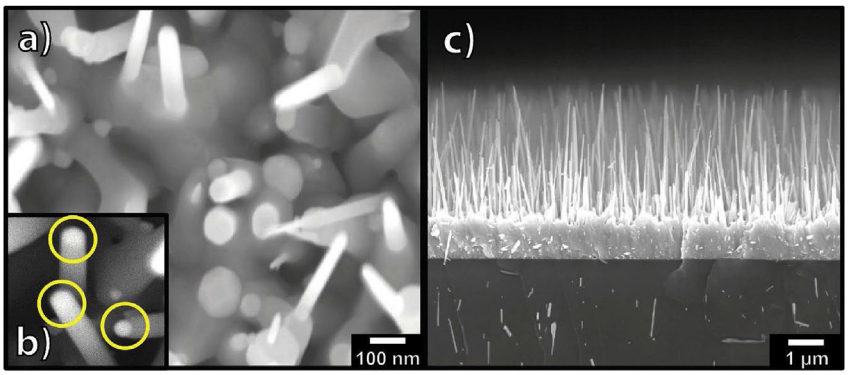

Fig. 7. SEM images of ZnO NWs grown on the sputtering-deposited seed layer (100,000x resolution): a) planar view (SEI detector), b) planar view (LEI detector) and c) cross-sectional view (SEI detector, 10,000X resolution).

Table 2
Composition (before and after NWs growth), refractive index, diameter, length and thickness (obtained via SEM and null ellipsometry) of the NW is presented.

Sample	Seed layer				NWs		
	η	t_{sem} (nm)	t_n (nm)	EDS (at. %)	EDS (at. %)	D (nm)	L (μm)
USP	2.00 (±0.12)	493 (±86)	512 (±66)	Zn: 48.3 O: 50.6 Al: 1.1	Zn: 50.6 O: 47.1 Al: 0.7 Au: 1.6	58.7 (±13.5)	1.6 (±1.0)
Sputtering	1.93 (±0.04)	872 (±42)	864 (±40)	O: 49.6 Zn: 49.7 Al: 0.7	Zn: 54.1 O: 43.9 Al: Au: 2.2	71.0 (±11.9)	3.1 (±0.4)

sample is lower than the detection limit. These differences observed in the chemical composition likewise support the idea of an influence of the technique employed to deposit the seed layer.

3.4. Optical properties

Table 2 also shows the results of null Ellipsometry characterization performed on AZO seed layers. Measurements were carried out at different locations of the sample before growing the ZnO NWs to know about the homogeneity of the sample. It can be observed that both samples presented a value near to the theoretical value $\eta = 2.003$. Hence, it can be inferred that well-defined compact AZO seed layers were obtained regardless of the deposition technique. However, at the same time it can also be observed that the sputtering-deposited seed layer shown better homogeneity around the sample in comparison to USP-deposited one. Additionally, in Table 2 the thickness of the seed layers have been shown. It can be observed that the values obtained from the Ellipsometry are quite similar to the ones obtained from SEM micrographs. USP seed layer has a mean thickness of 492.7 nm, while, sputtering one has a mean value of 872.7 nm. Compared to USP sample, the sputtered one showed better homogeneity in thickness. This can be related to high vacuum conditions employed in sputtering deposition technique. However, after growing the NWs it was not possible to carry out the ellipsometry measurements due to the dispersion observed from the sample.

In Fig. 8, PL spectra of samples is shown. It can be seen that both samples exhibited an intense green emission (GE) in the visible region and a less intense emission in the UV region as it was reported earlier [45], but via changing the pressure of oxygen during the deposition. In the present work, GE is commonly attributed to

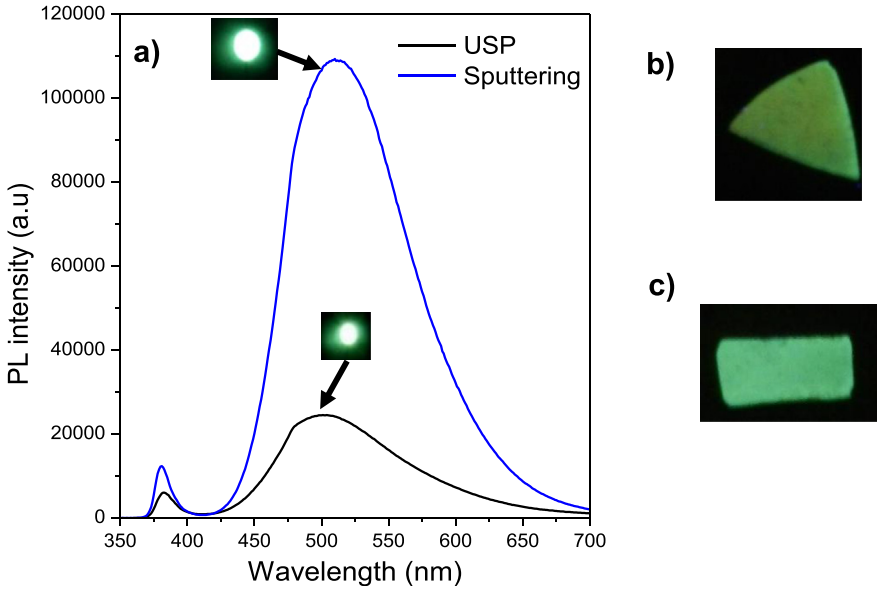

Fig. 8. (a), PL spectra of samples excited with a He-Cd laser at room temperature and samples excited with a UV lamp: b) NWs grown on the USP-deposited AZO seed layer and c) NWs has grown on the Sputtering-deposited seed layer.

intrinsic defects such as oxygen vacancies (V_o) and zinc vacancies (V_{zn}) and the luminescence origin is from the process of electron recombination in the singly ionized oxygen vacancy (V_o^{+}) with photo-excited holes in the valence band (VB) [46].

As well, it can be observed that the intensity of the visible emission in sputtered sample is higher than the USP one. Results obtained are in concordance with the EDS measurements. EDS results showed that the oxygen concentration in case of sputtered sample is lower as compared to the USP one. Furthermore, this could lead to the increase of V_o which could cause higher emission intensity. The intensity ratio of visible peak to UV (I_{vis}/I_{UV}) was demonstrated earlier in Ref. [47] to give some indication of the defect amount in ZnO samples.

In the present study, this ratio has values of 4.1 and 8.9 for USP and sputtered samples, respectively. Higher values of intensity ratio indicate a higher amount of defect sites. The present result is in concordance with the results obtained from XRD and EDS techniques supporting the idea of higher emission intensity due to oxygen vacancies. Furthermore, such an intense green emission observed at the room temperature could be used in the future for applications such as nano-photodetectors and nano-lasers.

4. Conclusions

The influence of the deposition method (USP and magnetron sputtering) on the formation of AZO as seed layer has been investigated. Furthermore, based on the seed layers structural, morphological and optical properties of ZnO NWs have been studied. Results show that the deposition technique employed for the development of AZO seed layer deposition has a strong influence on the structure and morphology of these layers and subsequently on the formation and properties of ZnO NWs. Together with XRD and SEM, it was found that the USP-seed layer showed better polycrystalline features with a (101) preferential growth compared to the sputtering-one that showed just one broad plane close to (002) direction. In comparison to the ZnO NWs grown by USP on the Au-covered seed layer, NWs on the sputtering-deposited seed layer showed a high-ordered orientation and vertical alignment. Samples obtained from both deposition techniques showed a stable, visible green emission under UV excitation. However, some differences in the emission intensity were also found. The higher intensity in the case of sputtered sample is in concordance with the emission related to defects, especially oxygen vacancies in the sample. Results revealed in the present work may shed some light on the orientation control and hence, emission of ZnO nanowires based on seed layers prepared by different techniques.

Acknowledgments

Author acknowledge to DGAPA PAPIIT for the projects IN108215 and IN107017 and CONACYT scholarships CVU-666934 and CVU-632376. Also, authors are indebted to Adriana Tejeda, Josué Esau Romero Ibarra, Carlos Ramos Vilchis and Cain Gonzalez, for their technical support in XRD, SEM and Lab measurements.

References

[1] J. Cui, Zinc oxide nanowires, Mater. Charact. 64 (2012) 43–52, http://dx.doi.org/10.1016/j.matchar.2011.11.017.
[2] Y.K. Mishra, V.S.K. Chakravadhanula, V. Hrkac, S. Jebril, D.C. Agarwal, S. Mohapatra, D.K. Avasthi, L. Kienle, R. Adelung, Crystal growth behaviour in Au-ZnO nanocomposite under different annealing environments and photoswitchability, J. Appl. Phys. 112 (2012), http://dx.doi.org/10.1063/1.4752469.
[3] S.V.N.T. Kuchibhatla, A.S. Karakoti, D. Bera, S. Seal, One dimensional nanostructured materials, Prog. Mater. Sci. 52 (2007) 699–913, http://dx.doi.org/10.1016/j.pmatsci.2006.08.001.
[4] S. Bok, R. Liu, J. Duay, S. Bok, Heterogeneous nanostructured electrode materials for electrochemical energy storage, Chem. Commun. 47 (2011) 1384–1404, http://dx.doi.org/10.1039/c0cc03158e.
[5] B.D. Fahlman, Nanomaterials, in: Mater. Chem., Springer, Netherlands, 2011, pp. 457–583, http://dx.doi.org/10.1007/978-94-007-0693-4_6.
[6] Ü. Özgür, D. Hofstetter, H. Morkoç, ZnO devices applications: a review of current status and future prospects, Proc. IEEE 98 (2010) 1255–1268, http://dx.doi.org/10.1109/JPROC.2010.2044550.
[7] S. Barth, F. Hernandez-Ramirez, J.D. Holmes, A. Romano-Rodriguez, Synthesis and applications of one-dimensional semiconductors, Prog. Mater. Sci. 55 (2010) 563–627, http://dx.doi.org/10.1016/j.pmatsci.2010.02.001.
[8] Ü. Özgür, Y.I. Alivov, C. Liu, A. Teke, M.A. Reshchikov, S. Doğan, V. Avrutin, S.J. Cho, H. Morko, A comprehensive review of ZnO materials and devices, J. Appl. Phys. 98 (2005) 1–103, http://dx.doi.org/10.1063/1.1992666.
[9] Z.L. Wang, Novel nanostructures and nanodevices of ZnO, zinc oxide bulk, thin film, Nanostructures (2006) 339–370, http://dx.doi.org/10.1016/B978-008044722-3/50010-5.
[10] M. Kumar, L. Wen, B.B. Sahu, J.G. Han, Simultaneous enhancement of carrier mobility and concentration via tailoring of Al-chemical states in Al-ZnO thin films, Appl. Phys. Lett. 106 (2015) 1–6, http://dx.doi.org/10.1063/1.4922732.
[11] Q. Zhang, C.S. Dandeneau, X. Zhou, G. Cao, ZnO nanostructures for dye-sensitized solar cells, Adv. Mater 21 (2009) 4087–4108, http://dx.doi.org/10.1002/adma.200803827.
[12] D. Panda, T.Y. Tseng, One-dimensional ZnO nanostructures: fabrication, optoelectronic properties, and device applications, J. Mater. Sci. 48 (2013) 6849–6877, http://dx.doi.org/10.1007/s10853-013-7541-0.
[13] S.K. Arya, S. Saha, J.E. Ramirez-Vick, V. Gupta, S. Bhansali, S.P. Singh, Recent advances in ZnO nanostructures and thin films for biosensor applications: review, Anal. Chim. Acta 737 (2012) 1–21, http://dx.doi.org/10.1016/j.aca.2012.05.048.
[14] Z.L. Wang, Zinc oxide nanostructures: growth, properties and applications, J. Phys. Condens. Matter 16 (2004) R829–R858, http://dx.doi.org/10.1088/0953-8984/16/25/R01.
[15] Y.-B. Hahn, Zinc oxide nanostructures and their applications, Korean J. Chem. Eng. 28 (2011) 1797–1813, http://dx.doi.org/10.1007/s11814-011-0213-3.
[16] K. Kalantar-zadeh, B. Fry, Nano fabrication and patterning techniques, in: Nanotechnology-enabled Sensors, Springer, US, 2008, pp. 135–210, http://dx.doi.org/10.1007/978-0-387-68023-1_4.
[17] W. Gao, Z. Li, Nanostructured transition metal oxides and their applications in composites, Phys. Prop. Appl. Polym. Nanocomposites (2010) 723–742, http://dx.doi.org/10.1533/9780857090249.4.723.
[18] Y. Zhang, M.K. Ram, E.K. Stefanakos, D.Y. Goswami, Synthesis, characterization, and applications of ZnO nanowires, J. Nanomater 2012 (2012), http://dx.doi.org/10.1155/2012/624520.
[19] K. Govatsi, A. Chrissanthopoulos, S.N. Yannopoulos, ZnO nanowires: growth, properties and advantages, in: P. Petkov, D. Tsiulyanu, W. Kulisch, C. Popov (Eds.), Nanosci. Adv. CBRN Agents Detect. Inf. Energy Secur., Springer, Netherlands, 2015, p. 21, http://dx.doi.org/10.1007/978-94-017-9697-2.
[20] D.R. Sahu, C.P. Liu, R.C. Wang, C.L. Kuo, J.L. Huang, Growth and application of ZnO nanostructures, Int. J. Appl. Ceram. Technol. 10 (2013) 814–838, http://dx.doi.org/10.1111/j.1744-7402.2012.02795.x.
[21] M. Willander, O. Nur, Q.X. Zhao, L.L. Yang, Zinc oxide nanorod based photonic devices: recent progress in growth, light emitting diodes and lasers, Nanotechnology 20 (2009) 332001, http://dx.doi.org/10.1088/0957-4484/20/33/332001.
[22] N.P. Dasgupta, J. Sun, C. Liu, S. Brittman, S.C. Andrews, J. Lim, H. Gao, R. Yan, P. Yang, 25th anniversary article: semiconductor nanowires - synthesis, characterization, and applications, Adv. Mater 26 (2014) 2137–2183, http://dx.doi.org/10.1002/adma.201305929.
[23] Y.K. Mishra, G. Modi, V. Cretu, V. Postica, O. Lupan, T. Reimer, I. Paulowicz, V. Hrkac, W. Benecke, L. Kienle, R. Adelung, Direct growth of freestanding ZnO tetrapod networks for multifunctional applications in photocatalysis, UV photodetection, and gas sensing, ACS Appl. Mater. Interfaces 7 (2015) 14303–14316, http://dx.doi.org/10.1021/acsami.5b02816.
[24] T. Reimer, I. Paulowicz, R. Röder, S. Kaps, O. Lupan, S. Chemnitz, W. Benecke, C. Ronning, R. Adelung, Y.K. Mishra, Single step integration of ZnO Nano-and microneedles in Si trenches by novel flame transport approach: whispering gallery modes and photocatalytic properties, ACS Appl. Mater. Interfaces 6 (2014) 7806–7815, http://dx.doi.org/10.1021/am5010877.
[25] J. Gröttrup, S. Kaps, J. Carstensen, D. Smazna, Y.K. Mishra, A. Piorra, C. Kirchhof, E. Quandt, R. Adelung, Piezotronic-based magnetoelectric sensor: fabrication and response, Phys. Status Solidi Appl. Mater. Sci. 213 (2016) 2208–2215, http://dx.doi.org/10.1002/pssa.201532924.
[26] C. Soldano, E. Comini, C. Baratto, M. Ferroni, G. Faglia, G. Sberveglieri, Metal oxides mono-dimensional nanostructures for gas sensing and light emission, J. Am. Ceram. Soc. 95 (2012) 831–850, http://dx.doi.org/10.1111/j.1551-2916.2011.05056.x.
[27] J.L. Gomez, O. Tigli, Zinc oxide nanostructures: from growth to application, J. Mater. Sci. 48 (2013) 612–624, http://dx.doi.org/10.1007/s10853-012-6938-5.
[28] Y.K. Mishra, S. Kaps, A. Schuchardt, I. Paulowicz, X. Jin, D. Gedamu, S. Freitag, M. Claus, S. Wille, A. Kovalev, S.N. Gorb, R. Adelung, Fabrication of macroscopically flexible and highly porous 3D semiconductor networks from interpenetrating nanostructures by a simple flame transport approach, Part. Part. Syst. Charact. 30 (2013) 775–783, http://dx.doi.org/10.1002/

ppsc.201300197.
[29] M. Ahmad, J. Zhu, ZnO based advanced functional nanostructures: synthesis, properties and applications, J. Mater. Chem. 21 (2011) 599, http://dx.doi.org/10.1039/c0jm01645d.
[30] X. Sun, M.S. Saha, Nanotubes, nanofibers and nanowires as supports for catalysts, in: J. Zhang (Ed.), PEM Fuel Cell Electrocatal. Catal. Layers Fundam. Appl., Springer, London, 2008, pp. 655–714, http://dx.doi.org/10.1007/978-1-84800-936-3_14.
[31] K.P. Jayadevan, T.Y. Tseng, One-dimensional ZnO nanostructures, J. Nanosci. Nanotechnol. 12 (2012) 4409–4457, http://dx.doi.org/10.1166/jnn.2012.6486.
[32] H.-J. Choi, Vapor-liquid-solid growth of semiconductor nanowires, in: G.-C. Yi (Ed.), Semicond. Nanostructures Optoelectron. Devices, Springer, Berlin Heidelberg, 2006, pp. 1–36, http://dx.doi.org/10.1007/978-3-642-22480-5_1.
[33] V.G. Dubrovskii, Vapor-Liquid-Solid growth of nanowires, in: Nucleation Theory and Growth of Nanostructures, Springer, Berlin Heidelberg, 2014, pp. 300–600, http://dx.doi.org/10.1007/978-3-642-39660-1.
[34] J.K. Hyun, S. Zhang, L.J. Lauhon, Nanowire heterostructures, Annu. Rev. Mater. Res. 43 (2013) 451, http://dx.doi.org/10.1146/annurev-matsci-071312-121659.
[35] Y. Zhao, C. Li, M. Chen, X. Yu, Y. Chang, A. Chen, H. Zhu, Z. Tang, Growth of aligned ZnO nanowires via modified atmospheric pressure chemical vapor deposition, Phys. Lett. A 380 (2016) 3993–3997, http://dx.doi.org/10.1016/j.physleta.2016.06.030.
[36] R. Bahramian, A. Moshaii, H. Eshghi, Effect of seeding modification of substrate on the growth and UV detection properties of ZnO nanowires, Mater. Lett. 179 (2016) 222–225, http://dx.doi.org/10.1016/j.matlet.2016.05.078.
[37] F. Falyouni, L. Benmamas, C. Thiandoume, J. Barjon, A. Lusson, P. Galtier, V. Sallet, Metal organic chemical vapor deposition growth and luminescence of ZnO micro- and nanowires, J. Vac. Sci. Technol. B 27 (2009) 1662–1666, http://dx.doi.org/10.1116/1.3137017.
[38] H.-C. Hsu, H.-M. Cheng, C.-Y. Wu, H.-S. Huang, Y.-C. Lee, W.-F. Hsieh, Luminescence of selective area growth of epitaxial ZnO nanowires and random-growth-oriented nanobelts, Nanotechnology 17 (2006) 1404–1407, http://dx.doi.org/10.1088/0957-4484/17/5/040.
[39] J. Lee, S. Lee, M.G. Choi, I.J. No, J. Ryu, N. Dabra, J.S. Hundal, D.Y. Jeong, Synthesis and photoluminescence properties of hydrothermally-grown ZnO nanowires on the aerosol-deposited AZO seed layer, Ceram. Int. 40 (2014) 10693–10698, http://dx.doi.org/10.1016/j.ceramint.2014.03.054.
[40] J. Song, S. Lim, Effect of seed layer on the growth of ZnO nanorods, J. Phys. Chem. C 111 (2007) 596–600, http://dx.doi.org/10.1021/jp0655017.
[41] M.L. Cui, X.M. Wu, L.J. Zhuge, Y.D. Meng, Effects of annealing temperature on the structure and photoluminescence properties of ZnO films, Vacuum 81 (2007) 899–903, http://dx.doi.org/10.1016/j.vacuum.2006.10.011.
[42] L. Znaidi, G.J. a. a. Soler Illia, S. Benyahia, C. Sanchez, a. V. Kanaev, Oriented ZnO thin films synthesis by sol–gel process for laser application, Thin Solid Films 428 (2003) 257–262, http://dx.doi.org/10.1016/S0040-6090(02)01219-1.
[43] J.S. Hur, S. Jang, D. Kim, D. Byun, Microstructure of intrinsic ZnO thin film grown by using atomic layer deposition, J. Korean Phys. Soc. 53 (2008) 3033–3037.
[44] J.A. Andrade-Arvizu, M.F. García-Sánchez, M. Courel-Piedrahita, F. Pulgarín-Agudelo, E. Santiago-Jaimes, E. Valencia-Resendiz, A. Arce-Plaza, O. Vigil-Galán, Suited growth parameters inducing type of conductivity conversions on chemical spray pyrolysis synthesized SnS thin films, J. Anal. Appl. Pyrolysis 121 (2016) 347–359, http://dx.doi.org/10.1016/j.jaap.2016.08.016.
[45] D. Zhang, C. Wang, F. Zhang, Oxygen pressure and measurement temperature dependence of defects related bands in zinc oxide films, Vacuum 85 (2010) 160–163, http://dx.doi.org/10.1016/j.vacuum.2010.05.005.
[46] M. Li, G. Xing, G. Xing, B. Wu, T. Wu, X. Zhang, T.C. Sum, Origin of green emission and charge trapping dynamics in ZnO nanowires, Phys. Rev. B - Condens. Matter Mater. Phys. 87 (2013) 1–8, http://dx.doi.org/10.1103/PhysRevB.87.115309.
[47] A. Mortezaali, O. Taheri, Z.S. Hosseini, Thickness effect of nanostructured ZnO thin films prepared by spray method on structural, morphological and optical properties, Microelectron. Eng. 151 (2016) 19–23, http://dx.doi.org/10.1016/j.mee.2015.11.016.